

# Chemical Reviews

Volume 84, Number 1 February 1984

## Electron Spin Echo Spectroscopy of Organic Triplets

TIEN-SUNG LIN

*Department of Chemistry, Washington University, St. Louis, Missouri 63130*

*Received April 18, 1983 (Revised Manuscript Received August 10, 1983)*

### Contents

I. Introduction	1
II. General Principles of the ESE Technique	2
III. Theory of Electron Spin Echo Envelope Modulation for a Triplet State	4
IV. Application to Triplets	6
A. Anthracene Triplets at Room Temperature	6
B. Photolysis of Diphenyldiazomethane	7
C. ESE Studies of Randomly and Partially Oriented Triplets	8
V. Dynamical Aspects	10
A. Field-Scan ESE: Time-Resolved EPR Spectra	10
B. Triplet Kinetics	11
C. Excitonic Motion	12
VI. Comparisons with Other Techniques: CW EPR, Transient EPR, ODMR, and ENDOR	13
A. Time-Resolved Studies	13
B. Hyperfine Structure Studies	13
VII. Concluding Remarks	14
VIII. References	14

### I. Introduction

Knowledge of the nature of the triplet state appears to be of vital concern to chemistry, biophysics, and biology. One of the important characteristics of the triplet state is its paramagnetic properties which have been actively investigated since the first successful electron paramagnetic resonance (EPR) study of the naphthalene triplet in durene crystals by Hutchison and Mangum in 1958.<sup>1</sup> Many reviews,<sup>2-7</sup> books,<sup>8,9</sup> and at least a few thousand research papers have been published on the paramagnetic properties of triplet states. Optical Zeeman spectroscopy, conventional EPR, optically detected magnetic resonance (ODMR) in zero or high field, electron spin echo (ESE), and spin locking techniques have been employed to study the paramagnetism of the triplet state of numerous organic molecules and biological systems. These magnetic studies have yielded the following useful information: triplet exciton structure, spin-orbit coupling, zero-field splittings (ZFS), hyperfine splittings (HFS), nuclear quadrupole interaction (NQI), triplet population and



Tien-Sung (Tom) Lin was born in Taiwan. He received his B.S. from Tunghai University (1960), M.S. from Syracuse University (1965), and Ph.D. from the University of Pennsylvania (1968). He spent 1 year as a postdoctoral fellow at Harvard University before he joined the faculty at Washington University, where he is now an Associate Professor of Chemistry. He was a scientist-in-residence at Argonne National Laboratory for 1 year (1980-1981). Professor Lin's interests are molecular spectroscopy and photochemistry of organic solids.

depopulation kinetics, and spin relaxation processes, which in turn provide us with intermolecular interactions, spin density distribution, bonding nature, geometry or conformation of the concerned triplet state, spin polarization, energy transfer, and the environmental effect in energy propagation processes.

In this review, I shall describe the utility of ESE spectroscopy and its application to the studies of organic triplets. Specifically, two new areas of research on the triplet state will be discussed in this review: (1) magnetic properties of triplet states at ambient or higher temperatures, or of extremely fast relaxing and short-lived species (on the order of 10  $\mu$ s), and (2) spin density distribution of organic triplets.

In the past, most of the magnetic resonance experiments of organic triplets were performed at low temperatures (77 K or lower). However, the photoexcitation dynamics of organic systems observed at low temperatures are very much different from those at high temperatures. For instance, the spin relaxation and

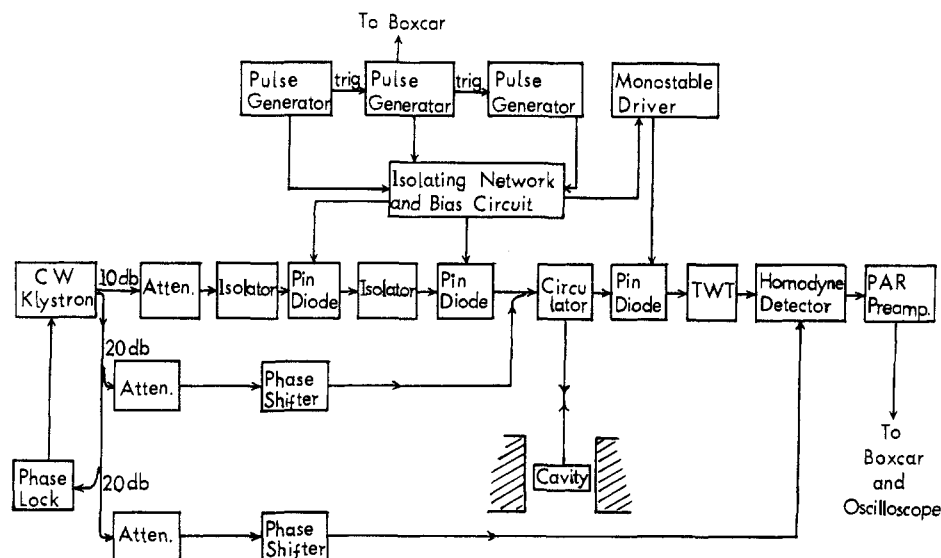


Figure 1. Simplified schematic diagram of the electron spin echo spectrometer at Washington University.

radiationless decay rates are always increased as the temperature is increased in higher temperatures regions. The lack of resonance studies at room or higher temperatures can be attributed mainly to the experimental difficulty in detecting weak and fast decaying signals (poor S/N ratio due to the fast spin-lattice relaxation and the diminished population difference between Zeeman levels at high temperatures). The paramagnetic properties of many short-lived triplets have been studied by the ODMR technique at low temperatures.<sup>3,5,9</sup> But the ODMR technique has not yet been developed for studying systems with extremely low triplet yield and/or with fast spin-lattice relaxation processes.

However, the organic triplet is often populated via a specific intersystem crossing pathway due to the selectivity of spin-orbit coupling. Thus, the spin polarization effect often prevails at the instant when the triplet is created. Electron spin polarization may also be produced by chemically induced dynamic electron polarization (CIDEP), as indicated in the EPR and ESE studies of <sup>2</sup>H *R. rubrum* triplets reported in ref 6 and 10. If one is able to capture the spin-polarized triplet before it relaxes to an equilibrium state, one would have a better chance in detecting the resonance signals arising from the paramagnetic species. Thus, it is possible to perform room temperature magnetic resonance experiments on organic triplets shortly after the excitation takes place and within the spin coherence time by employing a fast coherent detection scheme such as the ESE technique.

The information about the spin-density distribution of a great number of organic triplets are conspicuously missing in the literature. The lack of spin density information arises from the fact that resolvable HFS or electron nuclear double resonance (ENDOR) signals have been observed mostly in single crystal media. One should note that the triplet EPR lines in rigid glasses or powdered solids are seriously broadened due to the large ZFS and HFS anisotropies. This is in contrast to the doublet state where one can at least obtain the isotropic HFS, Fermi terms, in a liquid medium, and the spin-density distribution of a free radical may then be evaluated from the use of McConnell's relation. One should also note that the EPR spectra of organic triplets

can be observed only in rigid media, because the electron spin dipolar interaction of the triplet manifold in a liquid is averaged out to be 0. The single crystal requirement for mapping HFS of a triplet state by using the EPR or ENDOR technique therefore limits the feasibility of such studies to cases where suitable host crystals can be found.

The ESE technique is applicable to tackle these two areas of triplet research. The availability of pulsed-laser excitation, advanced microwave technology, and fast digitizing equipment have made the ESE technique a viable tool for such an application. The ESE technique is a pulsed-EPR experiment utilizing pulsed high microwave power. It is a time-domain spectroscopy. The fast detection scheme of ESE allows us to perform experiments on short-lived and fast relaxing triplets within the spin coherence time. The technique also allows us to study the coherence effect of nuclear spin states which is manifested in the periodic modulation of the electron spin echo decay envelope. This modulation effect can provide us with the information about the ENDOR frequencies. The technique can be applied to rigid glasses, to powdered solids, as well as to single crystal media. The technique is not restricted to the study of photoexcited triplet states, but also is applicable to the studies of ground-state triplets or biradicals, and of the spin polarization effect in photochemical processes.

Below I shall describe the general principles of the ESE technique and the underlying theory applicable to organic triplets. Results of some of our ESE experiments on triplets will be presented to demonstrate the utility of the technique for the study of organic triplets.

## II. General Principles of the ESE Technique

The general principles and experimental setup of ESE have been given in detail in ref 10-12. The schematic diagram of a typical ESE spectrometer used in our studies of organic triplets is displayed in Figure 1. The working principles of pulsed EPR are similar to those of pulsed NMR except for the working frequency, pulse duration, and the method of detection. The first condition is due to the fact that the gyro-

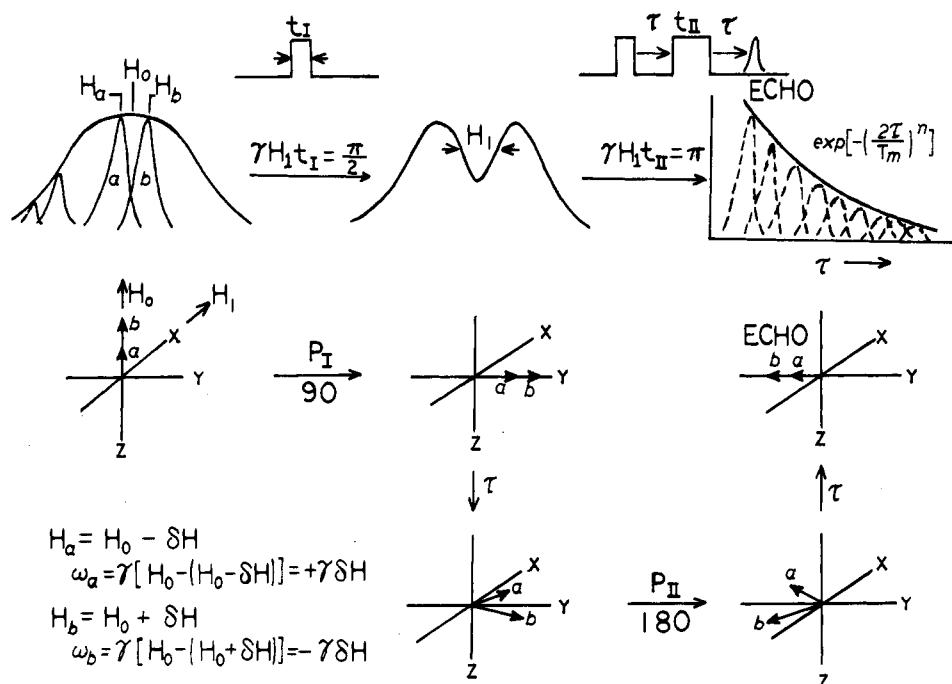


**Figure 2.** Overall views of hole burning, echo-formation, and echo-decay envelopes. Vector  $\mathbf{a}$  and  $\mathbf{b}$  represent the magnetization of the two spin packets.  $\omega_a$  is the free precession frequency of spin packet  $\mathbf{a}$  about the  $z$  axis in the rotating frame in the dephasing period, and  $T_m$  is the phase memory time.

magnetic ratio of the electron is about 200–1000 times greater than that of the nucleus. Thus, the working frequency is in the microwave frequency for pulsed EPR instead of the radio frequency for pulsed NMR. The pulse duration is determined by the following equation:

$$\theta = \gamma_{\text{eff}} H_1 t \quad (1)$$

where  $\theta$  is the tilt angle in radian,  $\gamma_{\text{eff}}$  is the effective gyromagnetic ratio,  $H_1$  the amplitude of the pulsed field, and  $t$  the pulse duration. We note that  $\gamma_{\text{eff}}$  for an  $S = 1$  system is  $2^{1/2}$  times that for an  $S = 1/2$  one, i.e., the effective rotation for  $S = 1$  is  $2^{1/2}$  times greater than that for  $S = 1/2$  (vide infra). For a typical  $\pi/2$  pulse,  $t$  is a few to about 100 ns in pulsed EPR vs.  $\mu\text{s}$  in pulsed NMR depending on the available amplitude of the  $H_1$  field. Due to the nature of line width in EPR and the availability of microwave intensity, pulsed EPR often detects echoes while pulsed NMR detects free induction decays (FID). For instance, if the EPR spectra of interest are inhomogeneously broadened lines with a width of about 40 G (typical linewidth for a randomly oriented triplets), the power required to burn a hole with an  $H_1$  field of 40 G is about 10 kw. A  $\pi/2$  pulse would have a duration of about 2 ns for an X-band spectrometer (9 GHz and  $Q \simeq 400$ ). The power and switching requirement and the deadtime associated with high microwave power would make the FID detection a difficult task in pulsed-EPR experiments. Thus, FID is often not a useful method in pulsed-EPR experiments, except for systems with narrow line width.

The most common pulse sequence used in pulsed-EPR experiments is two-pulse  $((\pi/2)-\tau-\pi)$ . The echo formation in a two-pulse experiment can be briefly described as follows: the first  $\pi/2$  pulse tilts the magnetization from the laboratory  $z$  axis to the  $x$  (or  $y$ ) axis, i.e., the  $\pi/2$  pulse produces the maximum transverse magnetization. Free precession of spin packets ensues after the removal of the microwave

pulse, i.e., dephasing. The application of a  $\pi$  pulse at a time interval  $\tau$  after the application of the  $\pi/2$  pulse will lead to realignment of the spin packets, i.e., refocusing. One then observes an echo at time  $\tau$  after the second pulse. Experimentally, a pair of repetitive intense microwave  $\pi/2$  and  $\pi$  pulses with an interval  $\tau$  being slowly increased is applied to the sample while the aperture in a boxcar integrator is simultaneously advanced to occur at time  $\tau$  following the second pulse. The dependence of the echo amplitude on  $\tau$  is the echo-decay envelope. Figure 2 illustrates the overall views of hole burning, echo formation, and echo-decay envelope.

The ESE decay envelope observed in a two-pulse experiment is given by  $A \exp[-(2\tau/T_m)^n]$  where  $T_m$  is the phase memory time, and  $n$  is a noninteger parameter which depends on the nature of local field fluctuation.<sup>11</sup> Often the  $T_m$  value is the limiting time in a two-pulse experiment.  $T_m$  is closely related to the familiar  $T_2$  of pulsed NMR. If  $T_m$  is shorter than or equal to the instrument deadtime (due to cavity ringing  $\sim 200$  ns), we cannot perform meaningful two-pulse ESE experiments. However,  $T_m$  is a function of temperature, solvent matrix, and spin concentration. Specifically,  $T_m$  is dictated by the local field fluctuation of the following two sources: (a) direct effect—spin flips of the echo-generating spin themselves; (b) indirect effect—disturbances in the environment which modify the Larmor frequencies, and thus randomize the phase of precession of each individual spin. The direct effect is important in systems of high spin concentration, while the indirect one is important in dilute spins. So a proper selection of experimental conditions may overcome the limitation due to  $T_m$ . Furthermore, a study of  $T_m$  as a function of concentration and temperature would enable us to gain some detailed dynamical information (see section V).

Another pulse sequence often used in the pulsed-EPR experiment is three-pulse  $((\pi/2)-\tau-(\pi/2)-T-(\pi/2))$ ,

where the time interval  $\tau$  between the first two  $\pi/2$  pulses is fixed, and the time  $T$  between the second  $\pi/2$  pulse and the third  $\pi/2$  pulse is varied. The echo forms at  $\tau$  after the third pulse. The echo formed in this pulse sequence is often called a stimulated echo. One may view the three-pulse sequence in terms of the  $((\pi/2)-\tau-\pi)$  series, where  $\pi$  is divided into two  $\pi/2$  pulses separated by a time  $T$ . Physically, the second  $\pi/2$  pulse preserves the transverse magnetization produced in the first  $\pi/2$  pulse and stores part of the magnetization along the  $z$  axis that can persist for a relatively long time (on the order of the spin-lattice time  $T_1$ ). The cycle of events can be continued by applying the third  $\pi/2$  pulse. In condensed media,  $T_1$  is often longer than  $T_m$  which then allows us to perform ESE experiments on systems with short  $T_m$  but long  $T_1$  by using the three-pulse sequence.

There are two pulse sequences often used to measure the spin-lattice relaxation times: (a) multiple pulse picket sequences—a  $(\pi-\tau'-\pi-\tau')$  sequence is applied for signal saturation followed after a time  $T_B$  by a two-pulse  $((\pi/2)-\tau-(\pi/2))$  echo series; (b) magnetization recovery sequence—a  $(\pi-T-(\pi/2)-\tau'-\pi)$  sequence where a  $\pi$  pulse switches  $+z$  magnetization to  $-z$  and is followed by a two-pulse echo detection series.

Even though ESE is a time-domain spectroscopy, we can also obtain ENDOR frequency spectra from the fast Fourier transform (FFT) of the echo-decay envelope. This is due to the fact that the envelope of ESE often shows a periodic modulation at frequencies that are identifiably related to resonance frequencies of nuclei present in the system. This is known as the electron spin echo envelope modulations (ESEEM). The effect is a result of coherent superpositions of hyperfine states in the resonant electron spin states. For a simple  $S = 1/2$  system interacting with paramagnetic nuclei, there are two prerequisites to induce the coherent superposition.<sup>10-13</sup> Firstly, the intensity of microwave  $H_1$  field must be comparable to or greater than the separation of nuclear Zeeman levels. Thus for  $H_1 = 10$  G, we can measure ENDOR frequencies up to 28 MHz. Since the tilt angle of the microwave pulse is given by eq 1, we may equivalently state that the pulse duration must be short in comparison with the reciprocal of ENDOR frequencies. Secondly, the directions of the effective field seen by nuclei in the two electron spin states must not be parallel to each other.

Let us see physically how these two prerequisites entail the observation of ESEEM: Upon the application of the first intense microwave pulse ( $\pi/2$ ) the electron spin undergoes reorientation which is a sudden event on the time scale of nuclear precession, and therefore produces a nonadiabatic change in the direction of the local field. The nuclei are no longer in stationary states and begin free precession after the removal of the first microwave pulse and during the dephasing period. This in turn leads to a periodic change in the local field seen by the electron and gives rise to an oscillatory echo envelope after the application of a refocusing pulse ( $\pi$ ).

The ESEEM observed in the two-pulse experiment contain not only the pure ENDOR frequencies but also the sums and differences of the nuclear frequencies. However, the ESEEM observed in three-pulse experiments give only the pure ENDOR frequencies.<sup>11,12</sup> Physically, one may view that the second pulse intro-

duces the sums and differences of the nuclear frequencies, and the third pulse causes these sums and differences to interfere and to leave only the pure ENDOR frequencies in the ESEEM observed in the three-pulse experiment. Furthermore, three-pulse ESEEM usually appear over a longer period than two-pulse ESEEM because of the extra time interval  $T$  introduces between the second and the third pulses. This longer modulation period gained in the three-pulse experiment is valuable in the accurate determination of lower nuclear frequencies. We shall demonstrate these effects in the analysis of ESEEM observed in diphenylmethylenes (section IVB).

The density matrix approach of the ESEEM of an electron spin ( $S = 1/2$ ) interacting with a proton is treated in ref 11-12. An elegant description of ESEEM has also been given in ref 10 and 13. The advantages, limitations, and sensitivity of the ESE technique have been reviewed in ref 10. With the availability of computer and fast digitizing equipment, we have observed ESE signals in a sample with a spin concentration as low as  $10^{13}$  cm<sup>-3</sup>. The sensitivity of ESE is therefore comparable to CW EPR.

### III. Theory of Electron Spin Echo Envelope Modulation for a Triplet State

The ESEEM of the photoexcited triplet state of quinoxaline,<sup>14</sup> of phenazine,<sup>15</sup> and of the ground triplet state of diphenylmethylene (DPM)<sup>16-18</sup> have previously been reported. However, no theoretical treatment of ESEEM of a triplet system has been given. In a recent publication, we have derived a theory so that we were able to simulate two-pulse ESEEM observed in pentacene triplets using the density matrix formalism.<sup>19,20</sup> Below we briefly summarize the essential theoretical treatment of ESEEM in a triplet state.

We shall consider one  $S = 1$  triplet interacting independently with isolated nuclei, each with  $I = 1/2$ . The spin Hamiltonian of a single  $S = 1$ ,  $I = 1/2$  system in an external field  $H_0$  is

$$\mathcal{H} = g\beta H_0 \cdot \mathbf{S} + \hbar D(S_z^2 - (1/3)S^2) + \hbar E(S_x^2 - S_y^2) - g_n \beta_n H_0 \cdot \mathbf{I} + \mathbf{S} \cdot \mathbf{T} \cdot \mathbf{I} \quad (2)$$

The electron  $g$  factor is assumed to be isotropic,  $D$  and  $E$  are ZFS with respect to the dipolar principal axes,  $T$  is the hyperfine tensor, and the other symbols have their usual meanings in magnetic resonance. The corresponding spin eigenfunctions in the high-field approximation can be written as follows:

$$\begin{aligned} | +1 \rangle \quad & |\psi_1\rangle = |\alpha_1\alpha_2\rangle(-b^*|\alpha_I\rangle + a^*|\beta_I\rangle) \\ & |\psi_2\rangle = |\alpha_1\alpha_2\rangle(a|\alpha_I\rangle + b|\beta_I\rangle) \\ | 0 \rangle \quad & |\psi_3\rangle = \frac{1}{\sqrt{2}}(|\alpha_1\beta_2\rangle + |\beta_1\alpha_2\rangle) |\beta_I\rangle \\ & |\psi_4\rangle = \frac{1}{\sqrt{2}}(|\alpha_1\beta_2\rangle + |\beta_1\alpha_2\rangle) |\alpha_I\rangle \\ | -1 \rangle \quad & |\psi_5\rangle = |\beta_1\beta_2\rangle(-d^*|\alpha_I\rangle + c^*|\beta_I\rangle) \\ & |\psi_6\rangle = |\beta_1\beta_2\rangle(c|\alpha_I\rangle + d|\beta_I\rangle) \end{aligned} \quad (3)$$

where  $\alpha_i$  and  $\beta_i$  ( $i = 1, 2$ ) are the electron spin functions,  $\alpha_I$  and  $\beta_I$  are nuclear spin functions, and  $a$ ,  $b$ ,  $c$ , and  $d$  are the branching parameters. The  $|0\rangle$  state does not have a first order HFI, so the energy separation between

$|\psi_3\rangle$  and  $|\psi_4\rangle$  is the nuclear Zeeman energy corresponding to the free nuclear frequency  $\omega_I$ . The frequency corresponding to the energy difference between  $|\psi_1\rangle$  and  $|\psi_2\rangle$  is

$$\omega_{+1} = [B^2 + (\omega_I - A)^2]^{1/2} \quad (4)$$

and that between  $|\psi_5\rangle$  and  $|\psi_6\rangle$  is

$$\omega_{-1} = [B^2 + (\omega_I + A)^2]^{1/2} \quad (5)$$

where  $A$  and  $B$  are terms in  $\hbar AS_z I_z + \hbar BS_z I_x$  of the HFI in the laboratory frame Hamiltonian.

The branching parameters can be expressed as follows:

$$a = \pm \frac{B}{[B^2 + (\omega_{+1} - \omega_I + A)^2]^{1/2}} \quad (6)$$

$$b = \mp \frac{\omega_{+1} - \omega_I + A}{[B^2 + (\omega_{+1} - \omega_I + A)^2]^{1/2}}$$

$c$  and  $d$  have similar expressions.

Below we show a general expression for the envelope modulation of the two-pulse ESE derived via the density matrix formalism.<sup>20</sup> The echo amplitude of the  $j$ th electron-nuclear spin pair at time  $2\tau$  can be calculated by evaluating  $\text{Tr}(\rho M_+)$  in the rotating frame as follows:

$$\text{Tr}(\rho M_+)_j = \text{Tr}(R_\tau R_{II} R_\tau R_I \rho_0 R_I^{-1} R_\tau^{-1} R_{II}^{-1} R_\tau^{-1} M_+) \quad (7)$$

where  $M_+ = M_x + iM_y$ ,  $R_\tau$  are the free precession operators that accumulate phase during the time  $\tau$  between the microwave pulses,  $R_I$  and  $R_{II}$  are nutation operators corresponding to the microwave pulses I and II, and  $\rho_0$  is the initial density matrix for the triplet population following the photoexcitation.

A microwave field can induce transitions between the two electron Zeeman levels when the magnetic field is set at resonance. The corresponding four eigenstates given in eq 3 are connected by the nutation operators  $R_I$  and  $R_{II}$  during the intense microwave pulse field. This establishes coherence among the four eigenfunctions. The time evolution of these eigenfunctions introduces interference effects which appear as modulations on the echo-decay envelope.

The operator  $S_y$  that connects the eigenstates in eq 3, e.g.,  $|\psi_1\rangle \leftrightarrow |\psi_3\rangle$  or  $|\psi_1\rangle \leftrightarrow |\psi_4\rangle$ , is related to a Pauli spin matrix  $\sigma_y$  by  $S_y = \sigma_y/2^{1/2}$ . We note that  $S_y = \sigma_y/2$  for a doublet system. Thus, the effective rotation for an  $S = 1$  system is  $2^{1/2}$  times that for an  $S = 1/2$  system.

After expanding the nutation operators of eq 7 by using the Cayley-Hamilton theory, we obtain the following expression for the echo-envelope modulation as a function of  $\tau$  for the  $|+1\rangle \leftrightarrow |0\rangle$  transition:

$$E(\text{mod}, \tau) = 1 - 2K \sin^2 \frac{\omega_{+1}\tau}{2} \sin^2 \frac{\omega_I\tau}{2} \quad (8)$$

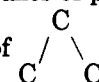
where

$$K = 4a^2b^2 = \left[ \frac{2B(\omega_{+1} - \omega_I + A)}{B^2 + (\omega_{+1} - \omega_I + A)^2} \right]^2 \quad (9)$$

Equation 8 is the same as Mims' expression for an  $S = 1/2$  system<sup>11</sup> except for the contents of the  $K$  term. The difference could arise from a true  $S = 1/2$  system with HF contribution in both the  $M_s = +1/2$  and  $M_s =$

$-1/2$  states, and a fictitious  $S = 1/2$  of the triplet system where one of the pair of the levels,  $M_s = 0$  has no HFS. For systems with large zero-field splittings, the contribution to ESEEM from the third triplet sublevel is negligibly small.

From eq 9, we note that the content of the  $K$  term determines the modulation pattern: if  $B = 0$ , then  $K = 0$ , and we would observe no ESEEM. In principle, we therefore do not expect to observe ESEEM arising from a particular set of protons in a molecule or biradical when the external field is parallel to the HF principal axes of protons which conventionally are the

bisector of  and along the C-H bond, normal to

the molecular plane, and normal to the above two axes. If the HF principal axes deviate from the above conventional axes, we should observe ESEEM even if the external field is parallel to the canonical axis. In fact, the ESE technique is a sensitive method to detect such discrepancies and to measure the  $B$  terms (off-diagonal HF tensor elements). This is demonstrated in the ESE studies of the triplet state of pentacene,<sup>19</sup> anthracene,<sup>21</sup> and tetracene.<sup>22</sup>

Analytically, in order to have a significant  $K$  value, one must have the following two conditions: (a)  $B \neq 0$ , i.e., off-diagonal HF tensor elements of some protons must not be 0, and (b)  $\omega_{+1} \simeq \omega_I \pm A$ , but not exactly equal, so the denominator in eq 9 is dominated by the  $B$  term.

Experimentally, in order to observe pronounced ESEEM, we must work at an intermediate external field, so that nuclear spins are not quantized along the external field. We do not want to work at an extremely high-field region, where both electron and nuclear spins are quantized along the external field. Another disadvantage of working at the high-field region is that the energy gap between nuclear levels then becomes very large which would then require a large  $H_1$  field and consequently a very short pulse duration to induce the coherence effect. This will certainly impose further technical difficulties. We also do not want to work at the zero-field where only the second-order HF interaction exists and the electron spin is quantized in the molecular principal axes. Overall, an intermediate field region, preferable 1 GHz or 300 G spectrometer, should be most suitable for triplet ESEEM studies. This is especially advantageous for a system with small HFI. However, the analysis and the interpretation of ESEEM could be messy, because one then has to solve the matrices exactly instead of using the high-field approximation. But this should not be too much of a problem. It is only a matter of computational details. We are currently in the process of setting up an 1-GHz pulsed spectrometer.

The observed modulation amplitudes are closely related to the branching parameters  $a$ ,  $b$ ,  $c$ , and  $d$  as given in eq 6 and 9. We may then express the diagonal HF element  $A$  and off-diagonal element  $B$  in terms of EN-DOR frequencies and branching parameters, for instance, for  $|\psi_1\rangle \leftrightarrow |\psi_2\rangle$

$$A = \omega_I - \omega_{+1} (1 - 2b^2) \quad (10)$$

and

$$B = \pm 2\omega_{+1}|a||b| \quad (11)$$

On the other hand, the observed ENDOR frequencies are related to the HF tensor elements. Thus, we should be able to establish a complete set of HF tensor elements from the observed modulation amplitude and the measured ENDOR frequencies. We can further calculate the spin density distribution from HF tensor elements. Below we shall discuss the application of the above outlined principles and theory of ESE spectroscopy to organic triplets.

#### IV. Application to Triplets

The first application of ESE to organic triplets is reported by Schmidt where he measured the rate of irreversible loss of coherence in the photoexcited triplet state of quinolines in durene crystals at 1.2 K in zero magnetic field.<sup>23</sup> Optically detected ESE in zero field in organic triplet has also been reported by Breiland et al.<sup>24</sup> Conventional ESE experiments (in a magnetic field) of the photoexcited triplets of quinoxaline,<sup>14</sup> naphthalene,<sup>14,25,26</sup> and pentacene<sup>27</sup> at liquid helium temperatures have been reported. Recently, we reported the ESEEM of pentacene,<sup>19</sup> anthracene,<sup>21</sup> and tetracene<sup>22</sup> triplets in *p*-terphenyl crystals at room temperature. An application of the ESE spectroscopy to study the nuclear quadrupole interaction of the photoexcited triplet state of phenazine has also been reported in the literature.<sup>15</sup> The ESE studies of ground-state triplets have been reported only on aromatic methylenes.<sup>16-18,28</sup> These ESE studies yielded significant information about the triplet state: assignments of ENDOR frequencies, NQI, spin relaxation time, spin polarization, nature of photochemical reaction, excitonic motions, and kinetic properties of spin sublevels at low temperatures.

Below we shall present some results of our recent triplet studies to illustrate the principle and the utility of the ESE technique: (A) room temperature studies of the phosphorescent state of anthracene in mixed crystals, (B) temperature-dependent studies of the photolysis of diphenyldiazomethane, and (C) measurements of ENDOR frequencies of triplets in randomly or partially oriented samples.

##### A. Anthracene Triplets at Room Temperature

Magnetic resonance studies of anthracene triplets have been reported previously.<sup>29-31</sup> All of these studies were performed at or below 77 K, except the EPR studies of neat anthracene crystals.<sup>31</sup> An ENDOR study of anthracene triplets in a phenazine crystal at liquid helium temperatures has been reported in ref 29. We performed our ESE studies of anthracene triplets in *p*-terphenyl crystals at room temperature.<sup>20,21</sup> The studies enable us to measure ENDOR frequencies from the FFT of ESEEM which can be used to evaluate the HF tensor elements and the spin density of anthracene triplets. Our studies were intended to make a comparative test of the capability of the ESE technique to map ENDOR frequencies of triplets at room temperature. Our experimentally measured lifetime of the anthracene triplet is about 40  $\mu$ s at room temperature vs. 40 ms at liquid helium temperature.

Typical room temperature ESE decay envelopes and the corresponding FFT of anthracene triplets in *p*-terphenyl crystals are displayed in Figure 3. The as-

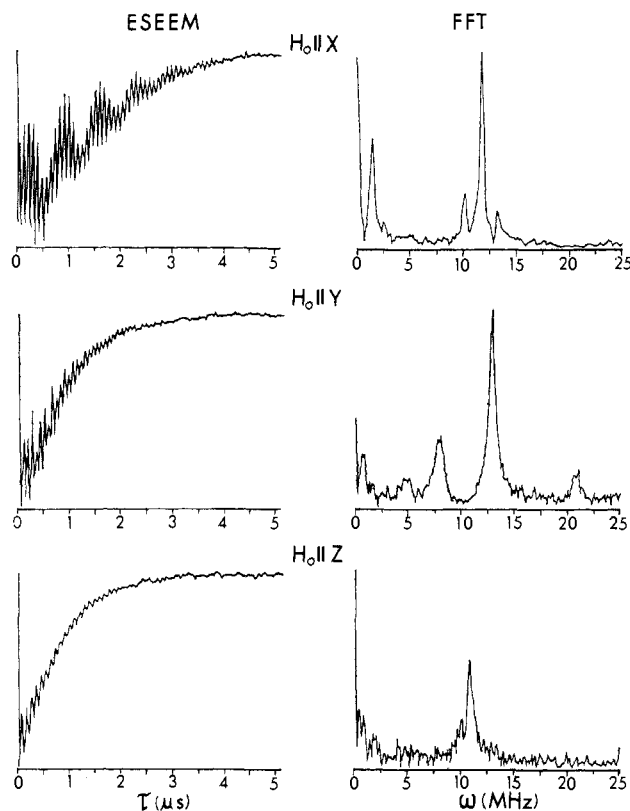


Figure 3. Two-pulse ESEEM and the corresponding FFT of the anthracene triplet in *p*-terphenyl crystals (low-field transitions) at room temperature.

signment of the observed frequencies were given in a previous publication.<sup>21</sup> Pronounced ESEEM appear only in the low-field resonance peaks (between  $|-1\rangle$  and  $|0\rangle$ ) of the two in-plane axes. There is little or no modulation on the corresponding high-field transition, i.e.,  $|+1\rangle \leftrightarrow |0\rangle$ . Physically, the appearance of modulation in the low-field transition but not in the high-field one indicates that the direction of the effective field seen by nuclei lies far away from the external field in the  $|-1\rangle$  manifold, while the effective field and the external field are almost parallel to each other in the  $|+1\rangle$  manifold.

By performing ESE experiments at three canonical orientations and a few off-axis orientations in three molecular planes of the anthracene molecule, we then have enough data to determine the HF tensor elements using a nonlinear least-squares-fitting program. The best fit HF tensor elements for protons of the triplet state of anthracene are given in Table I.<sup>21</sup> The results from the previous ENDOR studies<sup>29</sup> are also included in Table I. We note the following apparent differences:

(a) The  $A_{xy}$  elements of the  $\alpha$  and the meso protons: The ENDOR study gave a value of 0, whereas we have a value of +0.504 MHz for the  $\alpha$  and -0.354 MHz for the meso protons. The magnitude of  $A_{xy}(\alpha)$  relative to the difference between  $A_{xx}(\alpha)$  and the free proton frequency is significantly large, and thus gives rise to a large  $K$  value which determines the modulation depth (see eq 9). This is not quite so for the meso protons. Physically, we do expect  $A_{xy}(\alpha)$  to be non-zero due to the fact that the spin density at the meso carbons is much greater than that at the  $\beta$  carbons.<sup>29</sup> These differences in the spin density would induce differences in their dipolar interactions onto the  $\alpha$  protons. We should emphasize that it is the off-diagonal element

TABLE I. Best Fit Hyperfine Tensor Elements for the Anthracene Triplet (MHz)<sup>a</sup>

proton position <i>i</i>	this work			Clarke and Hutchison <sup>b</sup>		
	meso(9,10)	$\alpha(1,4,5,8)$	$\beta(2,3,6,7)$	meso(9,10)	$\alpha(1,4,5,8)^c$	$\beta(2,3,6,7)^c$
$A_{kxx}/h$	-26.02	-10.22	+1.34	-26.249	-10.512	
$A_{kyy}/h$	-7.85	-4.29	-5.14	-7.208	-3.250	
$A_{kzz}/h$	-18.03	-8.69	-4.65	-17.696	-8.643	-4.689
$A_{kxy}/h$	-0.354	+0.504	+2.05	0.000	0.000	
$A_{kxz}/h$	0	0	0	-0.211	-0.209	
$A_{kyz}/h$	0	0	0	0.000	0.000	

<sup>a</sup> The uncertainty in  $A_k$ 's is  $\pm 0.05$  MHz. <sup>b</sup> Reference 29. <sup>c</sup> Average value of the inequivalent protons, such as  $\alpha(1,5)$  and  $\alpha(4,8)$ .

TABLE II. Values of Spin Densities,  $\rho_i$  for the Anthracene Triplet

$\rho_i$	this work	Clarke and Hutchison <sup>a</sup>	Amos <sup>b</sup>	Hückel <sup>c</sup>
1,4,5,8	0.116	0.0986	0.085	0.0967
2,3,6,7	0.050	0.0792	0.029	0.0483
9,10	0.285	0.2498	0.324	0.1934
11,12,13,14	-0.058	-0.0527	-0.025	0.0083

<sup>a</sup> Reference 29. <sup>b</sup> Reference 32. <sup>c</sup> Reference 33.

$A_{xy}(\alpha)$  that gives rise to the observed ESEEM in the low field resonance peak of the  $x$  orientation.

(b) The tensor elements of the  $\beta$  protons: The ENDOR study gave only the  $A_{zz}$  element, whereas we have determined a complete set of elements. Our  $A_{zz}$  value is in good agreement with the ENDOR value. We should mention that the ENDOR study cannot observe any signals from the  $\beta$  protons except when the external field was parallel to the  $z$  axis, whereas we have observed modulations due to the  $\beta$  protons for  $H_0 \parallel y$  and for other off canonical orientations.

(c) The inequivalency of  $\alpha$  and  $\beta$  protons: The ENDOR study reported that elements for the  $\alpha$  protons at the 1- and 5-positions differ from those at the 4- and 8-positions, and  $\beta(2,6)$  differ from  $\beta(3,7)$ , while our study can not detect such differences. This may be due to a difference in the host matrix, phenazine vs.  $p$ -terphenyl, and the nature of two-pulse ESE experiments where the FFT (magnitude calculations) often introduce artificial linebroadening and thus obscure the finite difference in the appearance of spectral lines.

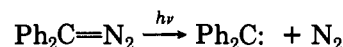
We have further evaluated the spin densities from the experimentally determined HF tensor using the standard procedure.<sup>20,29</sup> The values are tabulated in Table II. The values from the ENDOR study,<sup>29</sup> theoretically calculated values by Amos,<sup>32</sup> and those calculated by using simple Hückel MO coefficients<sup>33</sup> are also included in Table II.

We shall comment briefly on the differences among these sets of spin densities: Our best values re  $\rho_1 = 0.116$ ,  $\rho_2 = 0.050$ ,  $\rho_9 = 0.285$ , and  $\rho_{11} = -0.058$ . The simple Hückel calculation is not expected to give very good estimates of spin densities since it did not include electron correlation effect (e.g., the value for  $\rho_{11}$  should have been negative instead of 0.0083). The calculations of Amos<sup>32</sup> using unrestricted Hartree-Fock wave functions which are not eigenfunctions of  $S^2$  do not give good agreement with our measurements. The results of the ENDOR study of the anthracene triplet are probably inaccurate since the study did not yield enough data to determine a unique solution. There might also be a mistake in the assignments of the off-diagonal HF tensor elements of the  $\alpha$ -protons as mentioned earlier. We should mention that if we assigned

a wrong off-diagonal element to the  $\alpha$  protons, used the dipolar interaction in the C-H bond given in the ENDOR study, and neglected the HF tensor of  $\beta$  protons then we would obtain nearly the same results as that of the ENDOR study which gave a rather large spin density on the  $\beta$  protons:  $\rho_2 = 0.0792$ . This is much greater than our best result of 0.050. We should mention that the ENDOR value of  $\rho_2$  is also greater than both of the theoretical values given in Table II.

## B. Photolysis of Diphenyldiazomethane

This section will be concerned with the application of ESE to the study of the structural details of photo-products, specifically, diphenylmethylenes (DPM) and nitrogen molecules produced from the photolysis of diphenyldiazomethanes (DPDAM):



We shall describe the temperature dependence of this photochemical reaction. The ESE study of this system has been carried out in single crystal media and also in randomly oriented samples.<sup>18</sup> Previous low-power ESE studies of the system at liquid helium temperatures showed that the low modulation frequencies appearing in ESEEM could be attributed to the distant HFI of the trapped nitrogen molecules interacting with the nearby paramagnetic DPM.<sup>17</sup> The analysis further indicated that the quadrupole interaction (NQI) of  $\text{N}_2$  has been washed out due to a rapid tumbling.

We have employed a high-power ESE spectrometer ( $H_1 \approx 10$  G) to reexamine the photolysis of DPDAM. The objective of our study is to investigate the motion of trapped  $\text{N}_2$ . Specifically, we are concerned with the tumbling and the translational motion of  $\text{N}_2$  molecules as a function of temperature. We have employed perdeuterated DPDAM as a precursor in the study to differentiate the modulation frequencies between those due to  $^{14}\text{N}(I = 1)$  in  $\text{N}_2$  molecules and those due to protons in DPM. Figure 4A shows the ESEEM and their FFT spectra of DPDAM- $h_{10}$  and DPDAM- $d_{10}$  in benzophenone crystals after a brief irradiation at about 10 K. The samples were then warmed up to about 150 K momentarily, and cooled down to about 10 K again. The cooling down of the sample to 10 K was only to improve our S/N ratio and facilitate our analyses. The ESR decay envelopes of the annealed samples are shown in Figure 4B. Dramatically, all the modulations except those due to deuterons disappeared after the annealing. The annealing experiments confirm the assignments of previous ESE studies that the observed ESEEM are indeed due to  $^{14}\text{N}$  of the nitrogen molecule. The  $\text{N}_2$  molecules were frozen and trapped at the lattice sites right after the cleavage of the C=N<sub>2</sub> bond at 10

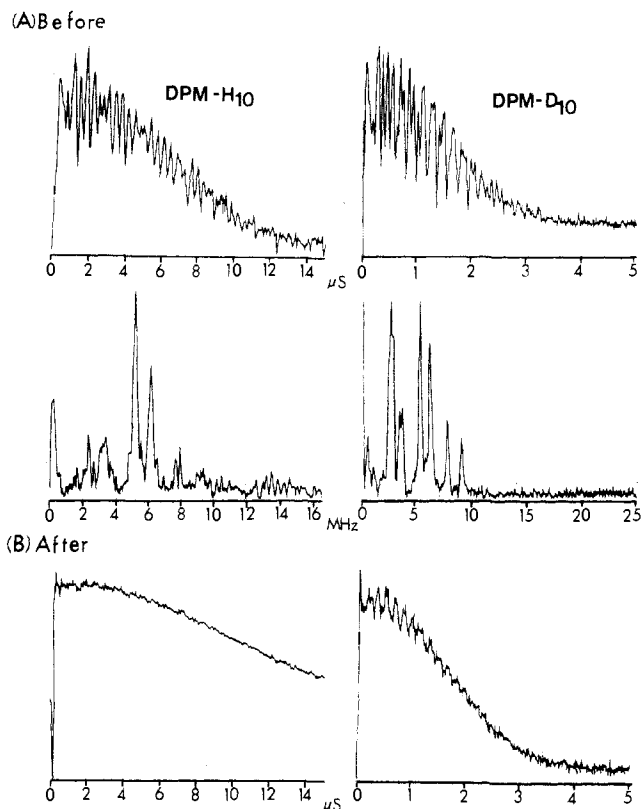


**Figure 4.** Two-pulse ESE decay envelopes of diphenylmethylene-*h*<sub>10</sub> and -*d*<sub>10</sub> ( $H_0 \parallel y$ ) before (A) and after (B) the sample was momentarily warmed up to 150 K. The echoes were taken at  $\sim 5$  K for DPM-*h*<sub>10</sub> and  $\sim 10$  K for DPM-*d*<sub>10</sub>. The middle spectra are the FFT of (A).

K. The analysis showed that the distance between <sup>14</sup>N nucleus and the divalent carbon of DPM along the pseudo-two-fold axis is  $2.5 \pm 0.7$  Å which is about twice that of the bond length of C=N in DPDM. Thus, the N<sub>2</sub> molecule has moved away from the divalent carbon by at least one bond length after the bond cleavage at  $\sim 10$  K. Upon thermalization, the N<sub>2</sub> molecule moves farther away from the divalent carbon and moves at least 10 Å away at 150 K and loses all the modulation effect. A precise measurement of temperature vs. ESEEM amplitude and frequency should give the detailed thermal history of this photochemical reaction.

Preliminary analyses of ESEEM showed that NQI of N<sub>2</sub> is not completely washed out at about 5 K. We obtained a magnitude of  $3.5 \pm 0.1$  MHz for  $3e^2qQ/4h$  and zero for the asymmetry parameter which are very similar to the results reported in the NQR study of <sup>14</sup>N in the  $\alpha$  phase of solid N<sub>2</sub>.<sup>34</sup> We note that the  $y$  axis is the pseudo-two-fold axis of DPM. The pronounced ESEEM observed in this orientation indicate that the HFI and/or NQI principal axes of <sup>14</sup>N are not aligned with the ZFS principal axes of DPM.

It would be instructive at this point to demonstrate the difference between two-pulse and three-pulse ESEEM. A series of three-pulse ESEEM and the corresponding FFT spectra for  $H_0 \parallel y$  (DPM-*d*<sub>10</sub>) at different  $\tau$  intervals is shown in Figure 5. We note the following: First, three-pulse ESEEM occur over a longer time scale than two-pulse ESEEM, and a better spectral resolution is observed in the lower frequency region in the FFT of three-pulse ESEEM (cf. Figure 4 and Figure 5). Second, the sums and the differences of ENDOR frequencies do not appear in three-pulse

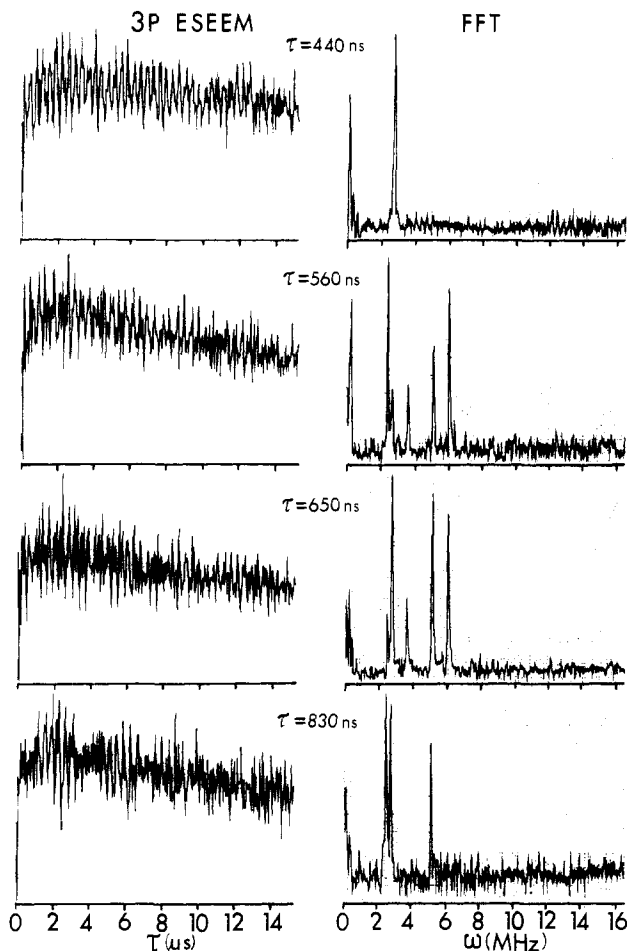


**Figure 5.** Three-pulse ESEEM and the corresponding FFT of diphenylmethylene-*d*<sub>10</sub> ( $H_0 \parallel y$ ) at different interspersal intervals at  $\sim 10$  K.

ESEEM, i.e., only peaks with fundamental ENDOR frequencies appear. For instance, the 9.0 MHz ( $= 3.7 + 5.3$ ) and the 7.8 MHz ( $= 2.5 + 5.3$ ) in Figure 4 disappear altogether in Figure 5. Third, a particular peak can be suppressed by a proper selection of  $\tau$ . For instance, for  $\tau = 440$  ns the 2.8 MHz appears to be the most intense peak, but for  $\tau = 560$  ns all frequencies appear strongly except the 2.8 MHz. A similar effect has been observed in the ESEEM of an  $S = 1/2$  system, and an explanation was explicitly given in ref 12.

In this fashion, one can further perform 2-D FFT which would facilitate the assignments of observed frequencies.

### C. ESE Studies of Randomly and Partially Oriented Triplets

So far we have only discussed triplets in single crystal media. Below we shall discuss disordered systems. The advantages of working with randomly oriented samples are two-fold: sample preparations are easy and simple, and almost all systems can be prepared either in rigid glasses or in powdered solids. Unfortunately, the EPR resonance peaks of randomly oriented triplets are very much inhomogeneously broadened and no resolvable HFS can be observed. The triplet EPR spectra of organic compounds in randomly oriented media display  $\Delta m = 2$  and  $\Delta m = 1$  transitions, and each of the  $\Delta m = 1$  transitions corresponds to a canonical orientation due to the magnetoselection effect. Thus, in principle,



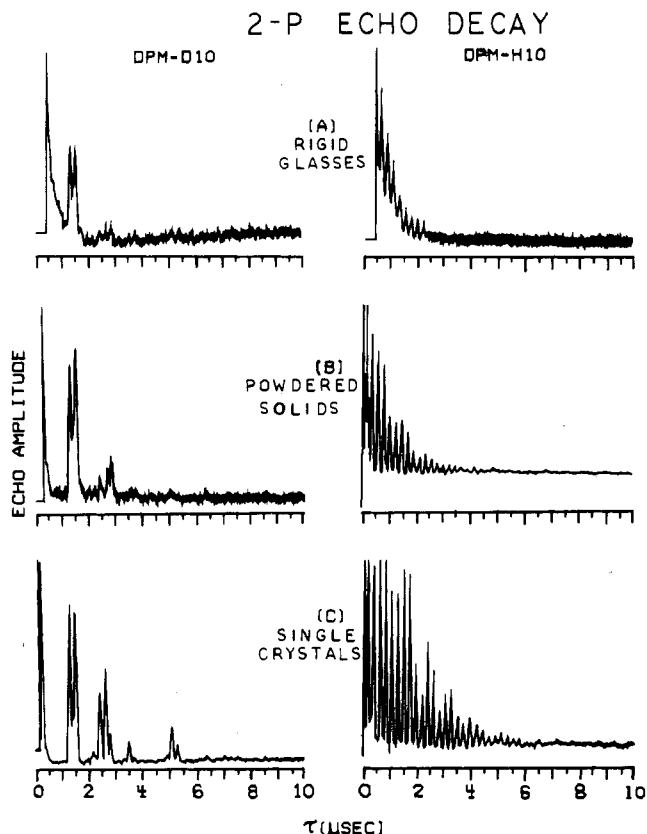


Figure 6. Two-pulse ESEEM of diphenylmethylenes in different forms of benzophenone at 5 K.

we should be able to perform ESE experiments of randomly oriented triplets at each of the canonical orientations. However, we should realize that the ESE signal to noise ratio in randomly oriented triplets will be definitely poorer than that in single crystal media under the same experimental conditions.

The ESEEM of DPM in benzophenone rigid glasses, polycrystalline solids, and single crystals are shown in Figure 6. The study showed that the modulation patterns of DPM at canonical orientations in disorder media are the same as those observed in single crystals except the amplitude of the echo-decay envelopes of DPM in rigid glasses diminish faster than those in powdered solids and single crystals, i.e., we lost some modulation information in the tail part of ESEEM when the triplet is in rigid glass media which consequently gives less information in the corresponding FFT spectrum (Figure 7). The observation indicates that  $T_m$  of DPM in single crystals and powdered solids are longer than that in rigid glasses. We also observed that  $T_1$  of the system depends greatly on the form of solids, longer  $T_1$  in single crystals and powdered solids. These differences in  $T_m$  and  $T_1$  in different forms of benzophenones could be attributed to cross relaxation due to the spread of Zeeman levels and/or hyperfine interactions. Also the low-lying quasi-continuum phonon states of rigid glasses may greatly affect  $T_1$ . On the other hand, the poorer resolution in rigid glasses and powdered solids may arise from overlapping of triplets with slightly different orientations.

Experimentally, we found that ESE signals of randomly oriented DPM appeared over a spread of several thousand gauss (1050–7580 G), most strongly at fields corresponding to canonical orientations, weaker at fields being 100–300 G off the canonical resonance fields.

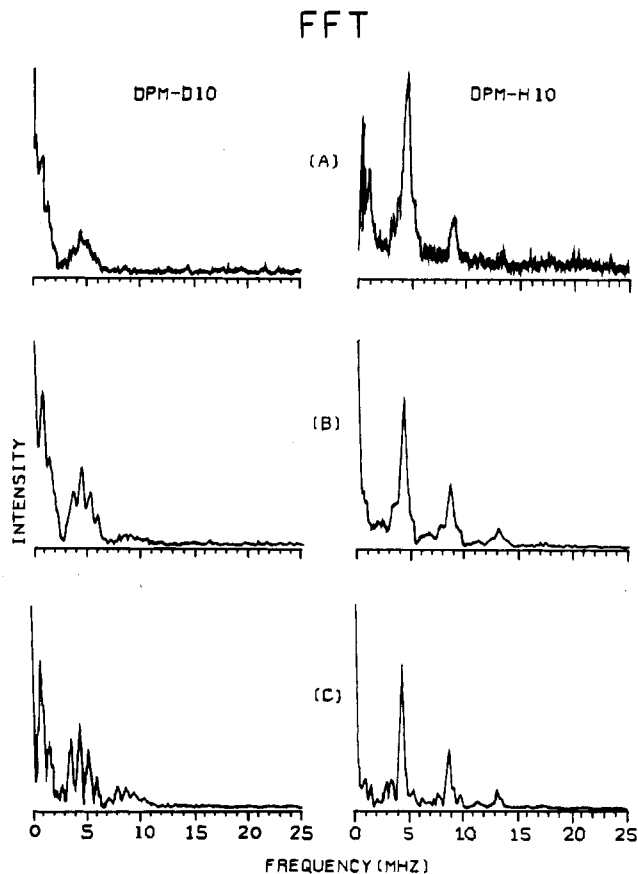
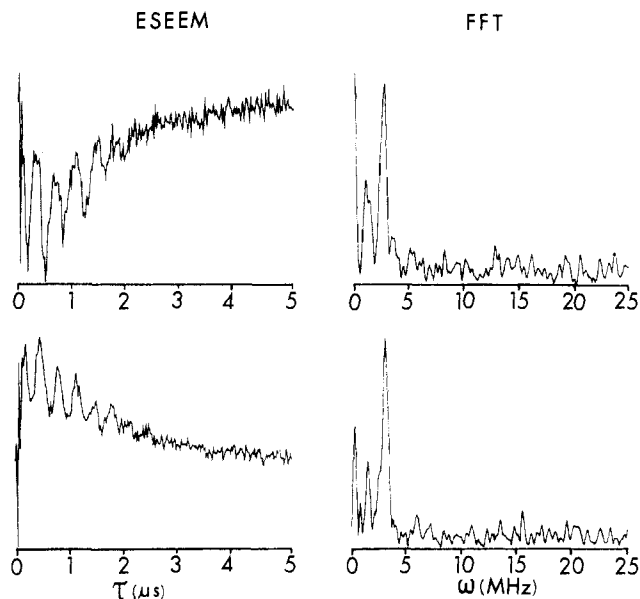


Figure 7. FFT spectra of ESEEM displayed in Figure 6.

This is in contrast with the CW EPR experiment of randomly oriented triplets, where signals appeared only at canonical resonance fields. This is due to the fact that the CW EPR peaks occur only at the special "turning" points (the first derivative is 0 or nearly 0 at points other than the turning points). On the other hand, the ESE technique does not yield a first derivative presentation but rather the magnetization itself. Thus a different magnetic field setting in ESE experiments of randomly oriented triplets should be sampling a particular set of molecular orientations. By performing ESE experiments at a different external field setting each time, one essentially can sample all possible orientations in randomly oriented sample, albeit with greatly diminished sensitivity.

The study of photoexcited triplet states in rigid glasses presents some problems in ESE experiments. The heat input from the excitation light source, especially from a xenon or mercury arc, is sufficient to shorten the  $T_m$ . To avoid the sample heating problem, we have employed a pulsed laser to excite the randomly oriented sample. To further improve the signal/noise ratio, one may disperse the molecules of interest in liquid crystals. The preparation of liquid crystal sample is almost as easy as that of powdered solids or rigid glasses except for the alignment of the liquid crystal sample. But this is still easier than the single crystal preparation. Furthermore, one can always find a proper liquid crystal to dissolve the molecule of interest.

Below we shall present results of some of our preliminary ESE studies on the photoexcited triplet state of zinc tetraphenylporphyrin (ZnTPP) in E-7 liquid crystals.<sup>35</sup> The partial molecular alignment in liquid crystals in the presence of a high magnetic field (8000



**Figure 8.** Two-pulse ESEEM and the corresponding FFT of zinc tetraphenylporphyrin triplets in E-7 liquid crystals for  $H_0 \parallel z$  at  $\sim 5$  K.

G) has enhanced the S/N ratio by about 1 order of magnitude in comparison with randomly oriented samples. Figure 8 shows the two-pulse ESEEM of ZnTPP excited by 532-nm green light from a Nd:YAG laser (Moletron MY32). The laser pulses are synchronized with the microwave pulses with or without delay. The corresponding FFT spectra are also given in Figure 8. It has been indicated that the plane of the macrocycle is aligned along the director of the liquid crystal, i.e.,  $H_0 \parallel L$  corresponds to the in-plane  $xy$  orientation.<sup>36</sup> We have also performed ESE experiments on ZnTPP- $d_{20}$  (deuterated phenyl rings) and we observed the same ESEEM spectra. Thus, the observed frequencies are not due to the protons of phenyl rings. It has been reported that the spin densities at the methine carbon positions of zinc porphyrin (ZnP) are 0.14, and those at nitrogens are 0.061 and 0.028.<sup>37,38</sup> If the orbital symmetry and the energy of ZnTPP triplet are similar to those of ZnP triplet, we would expect the spin density distribution to be similar in these two molecules. We thus tentatively assign the observed frequencies to nitrogens. The fact that we observed pronounced modulation due to nitrogen in the  $z$  orientation would imply the four nitrogens in the pyrrole rings of the macrocycle are not in the same plane in the photoexcited triplet state. Detailed analyses of the observed frequencies are in progress.

### V. Dynamical Aspects

Since the ESE signal is an event of tilting, dephasing, and refocusing of magnetization, we certainly can employ the ESE technique to follow the time evolution of photomagnetization. The advantages of the ESE technique over the CW EPR experiments are the response time which is about 200 ns (limited by cavity ringing deadtime) in ESE vs. about 100  $\mu$ s (limited by narrow bandwidths) in CW EPR, and the effect is nonequilibrium and nonlinear in ESE vs. steady state in CW EPR, i.e., the time evolution of magnetization in CW EPR is limited by  $T_1$  processes at high temperatures. The latter factor explains why all of CW

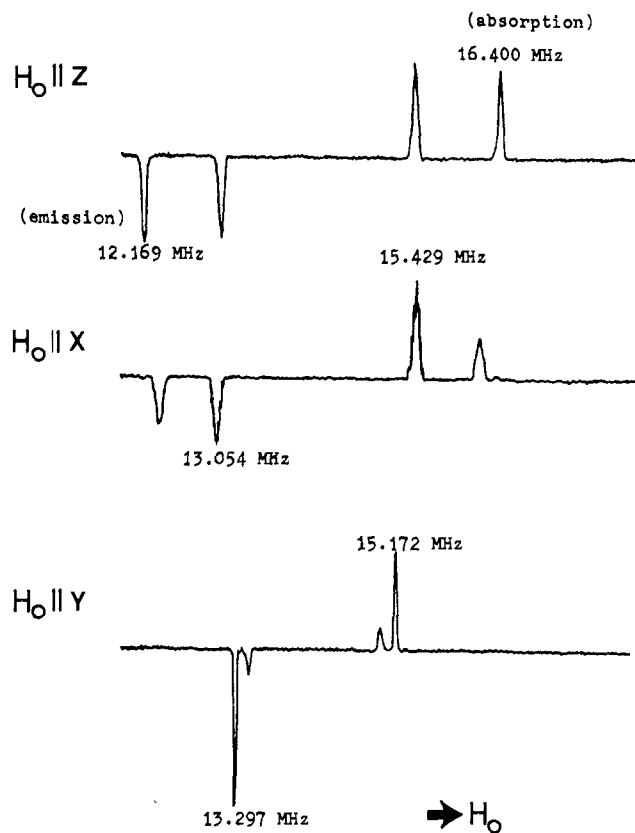


**Figure 9.** Field-scan ESE spectra of the pentacene triplet in the benzoic acid crystal at room temperature: (A)  $H_0 \parallel z$ , (B)  $H_0 \parallel x$ , (C)  $H_0 \parallel y$ . The  $H_1$  field is 0.5 G, microwave frequency is 9.4 GHz, and  $\tau$  is 2  $\mu$ s. The frequencies shown are measured from a proton magnetometer.

EPR of triplets have been performed at low temperatures where  $T_1$  is substantially lengthened. The fast response of the ESE technique allow us to perform the time-resolved studies of triplets even at room temperature.

### A. Field-Scan ESE: Time-Resolved EPR Spectra

The electron spin polarization effect occurring in the creation of triplet states can be followed in the ESE experiment. For photoexcited triplet states, field-scan ESE experiments produce time-resolved EPR spectra where the excitation laser pulses are synchronized with the microwave pulses and the spectra are recorded at the very beginning of the photoexcitation. Field-scan ESE experiments were performed by sweeping the magnetic field while fixing an appropriate time interval ( $\tau$ ) between two microwave pulses and having the aperture in the boxcar integrator opened at time  $\tau$  after the second microwave pulse. Figure 9 shows a set of typical field-scan ESE spectra of the photoexcited pentacene triplet in the benzoic acid crystal.<sup>20,39</sup> There is no time delay between the laser pulse and the first microwave pulse. The interval between the microwave pulses is 2  $\mu$ s, therefore the field-scan ESE spectrum represents the transient spectrum taken at 4  $\mu$ s ( $= 2\tau$ ) after the birth of the pentacene triplet. We observe only two pairs of signals that correspond to two magnetic inequivalent sites of the benzoic acid crystal. Since the ESE experiment measures the net magnetization of the spin system, the ESE spectrum gives the

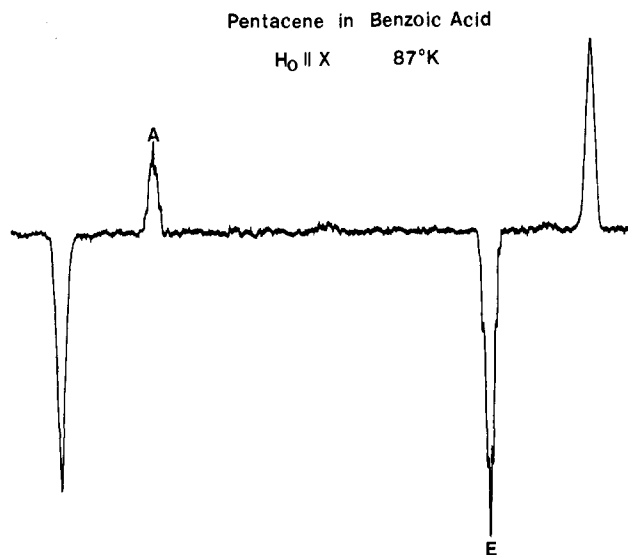


Figure 10. Field-scan ESE spectra of the pentacene triplet in the benzoic acid crystal at 87 K for  $H_0 \parallel x$ .

absorption intensity instead of the derivative one observed in CW EPR. We note that the low-field transitions displayed in Figure 9 are all in an emissive mode and the high-field ones are in absorptive mode. Note that the low-field transitions are  $| -1 \rangle \leftrightarrow | 0 \rangle$  for  $H_0 \parallel x$  and  $H_0 \parallel y$ , but  $| 0 \rangle \leftrightarrow | +1 \rangle$  for  $H_0 \parallel z$ . In the high-field approximation, the measured population rates can be related to the zero-field ones, e.g.,  $P_{+1} = P_{-1} = (P_y + P_z)/2$  for  $H_0 \parallel x$ . We can establish the relative zero-field population rates for the pentacene triplet as:  $P_x \approx P_y > P_z$ . Quantitative evaluations of  $P_i$  can be achieved in the fitting of kinetic curves (see section VB).

There is a dramatic change in the field-scan spectrum of the pentacene triplet for the  $H_0 \parallel x$  orientation when the sample temperature is lowered below 100 K (see Figure 10), where the low-field transition becomes absorptive and the high-field emissive. This is in contrast to the room-temperature spectrum. Apparently, the system undergoes a population inversion upon cooling. Detailed kinetic studies as a function of temperature indeed show such an effect (see below).

If the concerned triplet is not a photoexcited state, but rather a stable triplet (or biradical) produced from the photolysis of a precursor, the ESE technique is useful to study the spin polarization effect taking place in a photochemical reaction. For instance, Botter et al. have employed ESE to establish unambiguously the spin selectivity of DPM triplet generated from the photolysis of DPDAM upon laser irradiation.<sup>28</sup>

## B. Triplet Kinetics

The kinetics of the triplet population, decay, and relaxation rates can be easily examined by the ESE technique. The following experimental procedure is used in our kinetic studies: (1) Create the triplet state using a laser pulse, (2) apply the first microwave pulse ( $\pi/2$ ) after the laser pulse at a variable time interval of  $T_L$ , (3) apply the second microwave pulse ( $\pi$ ) after the  $\pi/2$  pulse at a fixed interval of  $\tau$ , and (4) detect the echo at  $2\tau$  after the first microwave pulse. By recording the echo height as a function of time  $T_L$ , we obtain the complete time evolution of photomagnetization. Essentially, each laser shot at a different delay time is

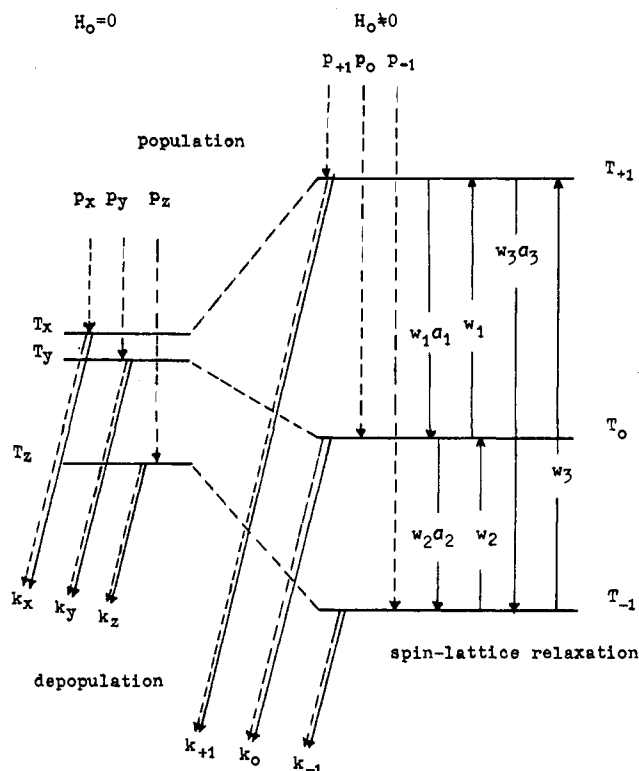


Figure 11. Kinetics of triplet excitation.

TABLE III. Best Fit of the Kinetic Parameters for Pentacene Triplet in *p*-Terphenyl and Benzoic Acid at Room Temperature<sup>a</sup>

	$P_0$	$P_{z1}$	$k_0$	$k_{z1}$	$w_1^b$	$w_2$	$w_3^c$
	$H_0 \parallel z$						
PHT <sup>d</sup>	0.10	0.45	1.0	14.5	18.5	26.3	6.6
PDT <sup>e</sup>	0.16	0.42	1.0	7.2	17.7	28.6	7.5
PHB <sup>f</sup>	0.22	0.39	9.9	16.0	30.4	29.2	20.5
	$H_0 \parallel x$						
PHB	0.44	0.28	14.5	7.4	13.7	7.8	4.9

<sup>a</sup> Units for  $k_i$  and  $w_i$  are  $10^3 \text{ s}^{-1}$ . <sup>b</sup>  $w_1$  is the spin-lattice relaxation rate for  $| 0 \rangle \leftrightarrow | +1 \rangle$  transition. <sup>c</sup>  $w_3$  is for  $| -1 \rangle \leftrightarrow | +1 \rangle$  transition. <sup>d</sup> PHT, pentacene- $h_{14}$  in *p*-terphenyl. <sup>e</sup> PDT, pentacene- $d_{14}$  in *p*-terphenyl. <sup>f</sup> PHB, pentacene- $h_{14}$  in benzoic acid.

probing the status of the triplet born at that particular time lag. The kinetics of triplet excitation, schematically displayed in Figure 11, is governed by a set of following differential equations:<sup>20</sup>

$$\frac{dN_1}{dt} = -(w_1\alpha_1 + w_3\alpha_3 + k_1 + P_1)N_1 + (w_1 - P_1)N_0 + (w_3 - P_1)N_{-1} + P_1N_T$$

$$\frac{dN_0}{dt} = (w_1\alpha_1 - P_0)N_1 - (w_1 + \alpha_2w_2 + k_0 + P_0)N_0 + (w_2 - P_0)N_{-1} + P_0N_T$$

$$\frac{dN_{-1}}{dt} = (w_3\alpha_3 - P_{-1})N_1 + (w_2\alpha_2 - P_{-1})N_0 - (w_3 + w_2 + k_{-1} + P_{-1})N_{-1} + P_{-1}N_T$$

$$N_T = N_S + N_1 + N_0 + N_{-1} \quad (12)$$

where  $N_i$  is the population of the sublevels,  $\alpha_i$  the Boltzmann factor,  $w_i$  the spin-lattice relaxation rate,  $P_i$  the population rate, and  $k_i$  the depopulation rate.

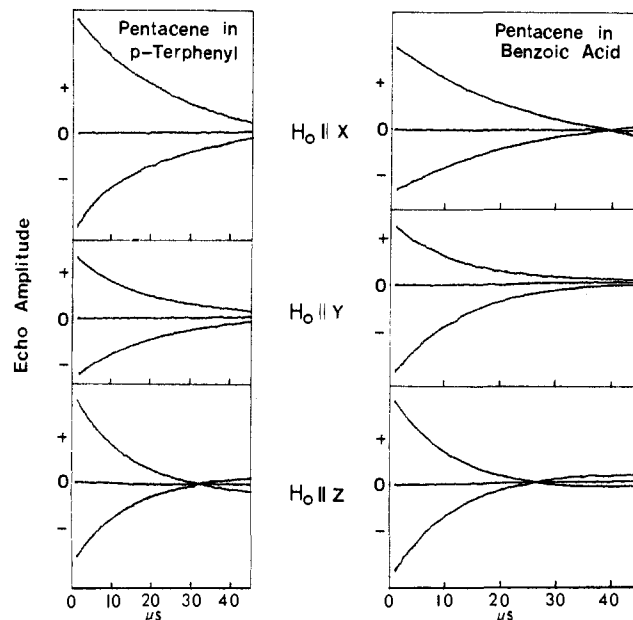


**Figure 12.** Echo-decay curves (echo amplitude vs. time delay from laser pulses) of the pentacene triplet in the *p*-terphenyl and the benzoic acid crystals at room temperature.

The decay curves of pentacene triplets in the benzoic acid host crystal and in the *p*-terphenyl crystal at room temperature are displayed in Figure 12. Table III gives the best fit kinetic parameters derived from these curves. Interestingly enough, the kinetic parameters of pentacene triplets in benzoic acid crystals are different from those in *p*-terphenyl crystals.<sup>19,20,39</sup> One noticeable effect is that the decay curve of pentacene in benzoic acid at room temperature with  $H_0 \parallel x$  changes sign at about  $39 \mu\text{s}$  where the decay curve of pentacene in *p*-terphenyl does not change sign at all in this field orientation. These results clearly demonstrated that the host crystal plays an important role in the triplet spin dynamics. The observed effect in the benzoic acid crystal may arise from the dynamical effect of the crystal, i.e., proton transfer in the benzoic acid dimer, and possibly from the heavy atom effect (oxygen in the benzoic acid) on the intersystem-crossing processes of the pentacene molecule.

As we mentioned in the field-scan ESE section, the *x* orientation of the pentacene triplet in the benzoic acid crystal showed a population inversion at low temperatures. Furthermore, the kinetic curve for  $H_0 \parallel x$  showed that the system undergoes the population inversion even at room temperature. We therefore took one step further to study the temperature effect on the triplet kinetics of the pentacene in the benzoic acid crystal, especially the *x* orientation.<sup>20,39</sup> The kinetic curves as a function of temperature for the high-field resonance line of the *x* orientation are displayed in Figure 13. We note that the initial echo signal underwent a drastic changeover when the sample temperature was lowered below 103 K. The time elapsed for the occurrence of the population inversion becomes shorter as the temperature decreases. Finally, at a temperature of 103 K, it no longer appears as an absorption even at  $t = 0$ , i.e.,  $P_0$  becomes less than  $P_{+1}$  or  $P_{-1}$  at time 0. There is no such drastic change for  $H_0 \parallel z$  in either the *p*-terphenyl or the benzoic acid crystal. The change in the initial population is more clearly brought out in the field-scan ESE spectra at low temperatures as mentioned earlier

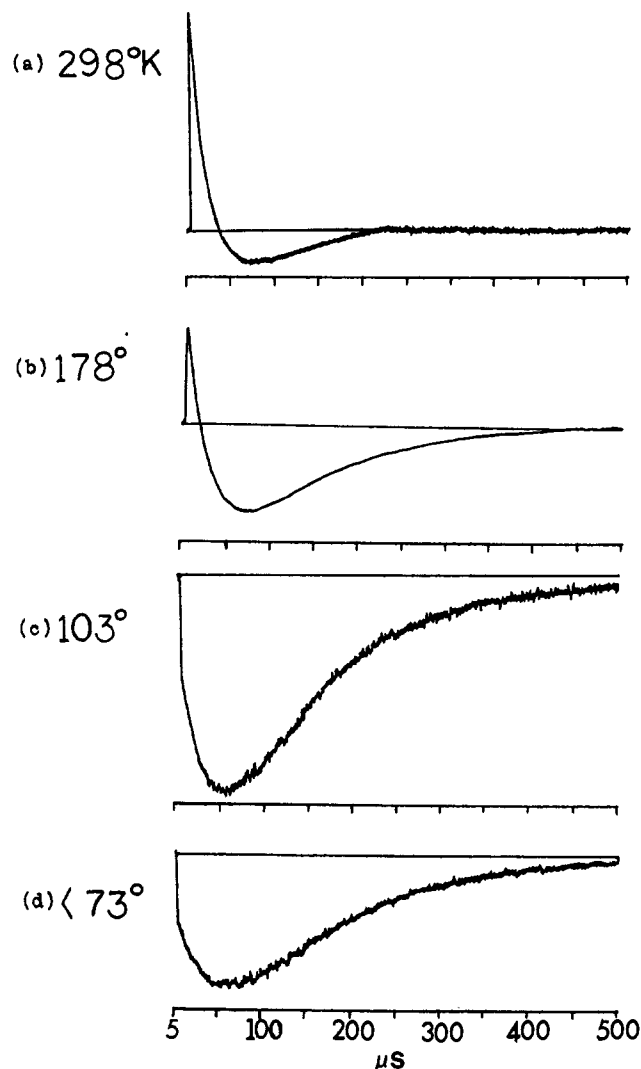


**Figure 13.** Kinetic curves of the pentacene triplet in the benzoic acid crystal as a function of temperature for the high-field resonance line of the *x* orientation.

(see Figure 10). The effect of temperature on the population scheme of the pentacene triplet in the benzoic acid crystal could arise from the changes in the rate of proton transfer and relative population of the two different dimeric configurations of the benzoic acid dimer. As the temperature is lowered, one of the tautomers becomes more stable and provides different environment for the pentacene molecule, especially the two in-plane axes. Thus the decrease in the population of the  $|X\rangle$  sublevel upon cooling may arise from a result of population redistribution to  $|Y\rangle$  substate due to possibly the change of site symmetry in the tautomerization.

### C. Excitonic Motion

In neat crystals or concentrated triplet spin systems, the triplet-triplet migration often is in effect. The spin dynamics of naphthalene dimers has been studied by Schmidt and van der Waals using the ESE technique.<sup>7,25-27</sup> They have examined the "mini-exciton" dynamics with regard to the interaction between exchange equivalent pairs (A-B), and between translationally equivalent pairs (A-A). The study of the spin dynamics in dimeric or aggregated systems has yielded not only the dynamical features of interacting triplets, but also

some structural information (such as relative configuration and the distance of interacting pairs). The triplet energy migration will affect the local field fluctuation and reflects in the observed  $T_m$ . It is believed that the exchange interaction ( $J$ ) is responsible for the triplet energy migration. To put the description of interacting triplets (between chemically identical molecules) in a better perspective, we write the corresponding eigenstates for an interacting pair as follows

$$\Psi_{\pm} = \frac{1}{\sqrt{2}}[|B_1^*B_2\rangle \pm |B_1B_2^*\rangle] \quad (13)$$

where  $|B_1^*B_2\rangle$  is the product state with molecule  $B_1$  in the triplet state and  $B_2$  in the ground state. If the interacting pair can be described by the eigenstates  $\Psi_+$  and  $\Psi_-$ , the system is a coherent one (an exciton or supermolecule model). If the excitation hops stochastically between two molecules, the system is in an incoherent limit (a hopping model).

However, the phonons in a real system will intervene with migration. At room temperature the distinction is determined by the relative magnitude of the exchange interaction  $J$  and the jumping rate  $W$  between the two states  $\Psi_+$  and  $\Psi_-$ . The jumping is a thermal process introduced by phonons. The excitation is coherent if  $W \ll 2J$ , and it is incoherent if  $W \gg 2J$ .<sup>7</sup> If one measured  $T_m$  as a function of temperature, one can evaluate the  $J$  value. The lifetime of the higher lying state and the jumping rate can be evaluated from the study of the shift of resonance frequencies as a function of temperature. One therefore can establish the nature of triplet migration.

The significance and the implication of the time-resolved studies of organic triplets in neat or nearly neat crystals are the following: first, the experimentally measured  $T_m$  value is a measure of the homogeneous magnetic resonance line width. By the application of the uncertainty principle, the inverse of the homogeneous line width determines the coherent lifetime of the supermolecule in a given set of energy levels. Second, the exchange interaction  $J$  value evaluated from the ESE experiment could in principle yield the distance and geometry of the interacting pair. Third, the jumping rate  $W$  is temperature dependent, and it is the relative magnitudes of  $W$  and  $J$  that determines the dynamics of energy migration. When the temperature of a system changes, a coherent system at very low temperature could change over to an incoherent one at high temperatures. Thus, at certain temperatures where  $W \approx 2J$ , the excitation begins to hop stochastically, and the exciton dynamics would not exist anymore.

## VI. Comparisons with Other Techniques: CW EPR, Transient EPR, ODMR, and ENDOR

Many other magnetic resonance techniques have been employed in the studies of organic triplets, such as CW EPR, transient EPR, ODMR, and ENDOR. Each of these techniques has its own advantages and shortcomings. Below I shall attempt to compare the utilities of each of these techniques and its applicability to the following two particular areas of triplet studies.

### A. Time-Resolved Studies

The time resolution of conventional CW EPR is about 100  $\mu$ s, limited by the field modulation built in the spectrometer, usually 100 KHz. Thus, CW EPR is not suited for probing a system with short-lived triplet or with fast relaxation processes.

Transient CW or pulsed EPR technique is in principle good for time-resolved studies. In the transient CW EPR experiments, the signal is detected directly at the diode using a wide-band amplifier. The signals of several millivolts, usually 5–10 times greater than the noise at the diode, are easily observed by watching the output of the diode on an oscilloscope triggered by the excitation laser pulse.<sup>40</sup> The signals may be captured on an appropriate transient digitizer following a single pulse or averaged over the necessary number of repetition in a signal averager interfaced to the digitizer. This technique provides enough sensitivity to study the time dependence of triplet dynamics even at room temperature. The time resolution is limited by the bandwidth of the amplifier used. It was found that a bandwidth of 1 MHz gave the best S/N ratio.

ODMR is also good for time-resolved studies provided that the changes in optical intensity induced by the applied microwave is detectable. It is a severe problem in ODMR experiments to detect signals arising from a triplet system with fast relaxing processes either due to the thermal effect or nonradiative decay. For instance, ODMR failed to detect signals of pentacene triplets even at liquid helium temperatures,<sup>41</sup> while transient CW EPR<sup>42</sup> and ESE technique<sup>19</sup> measured easily the magnetic properties of pentacene triplets at room temperature. Also the highest temperature performed in ODMR experiments was reported to be the boiling liquid nitrogen.<sup>9</sup> No room temperature ODMR of triplets has been reported in the literature.

The ESE technique, one form of pulsed EPR, has its limitation too. It has a time resolution of about 200 nsec limited by the cavity ringing depending on the magnitude of  $H_1$  field and cavity  $Q$  value. Recent developments in bimodal cavity design and the use of a microwave delay line have succeeded in reducing the instrument deadtime by 50%.<sup>43</sup>

### B. Hyperfine Structure Studies

The hyperfine splittings are a result of the interaction of electron spins with nuclei spins. The CW EPR and ODMR techniques are capable of displaying hyperfine splittings only when the splittings are greater than the line width and only in single crystal environment. This is due to the fact that the EPR hyperfine structure has as many as  $2^n$  lines for  $n$  inequivalent nuclei with  $I = 1/2$ . These lines often overlap very badly and form a rather broad band. Also the zero-field ODMR experiment can only detect the second-order hyperfine effect, but it can work with randomly oriented samples.

The situation is different in ENDOR experiments. The ENDOR spectrum is obtained by monitoring the EPR resonance as a function of radio frequency. We may think of ENDOR spectrum as NMR spectrum of the triplet using an EPR transition as a detection system. Furthermore, each nucleus gives only two nuclear resonance frequencies, i.e., one in each electron manifold (in  $M_s = +1$  and  $M_s = 0$  for  $|0\rangle \leftrightarrow |+1\rangle$  transition,

and in  $M_s = -1$  and  $M_s = 0$  for  $|0\rangle \leftrightarrow |-1\rangle$ ). There is no first-order HFI in the  $M_s = 0$  manifold. Therefore one observes a maximum of  $2n$  ENDOR lines instead of  $2^n$  EPR lines for  $n$  inequivalent nuclei with  $I = 1/2$ . The reduction in the number of spectral lines gives rise to a far better spectral resolution for ENDOR than for EPR. However, the ENDOR signal is observed through the desaturation of an EPR transition by inducing nuclear transitions, therefore the complicated balance of relaxation processes plays an important role in the ENDOR technique which is often a limiting factor in ENDOR measurements. To enhance the S/N ratio, most of the ENDOR experiments on organic triplets have been performed in single crystal environment and at very low temperatures (at 4.2 K or below). Also ENDOR are often not obtainable for orientations which are off the principal axes of hyperfine interaction tensors.

As we have presented above, the FFT of ESEEM gives the corresponding ENDOR frequencies. In contrast to the ENDOR technique, the ESE envelopes always show deep modulation for off-principal axes and little or no modulation for canonical orientations. So ESEEM is a valuable supplement to ENDOR. Furthermore, ESEEM allows us to map ENDOR frequencies of organic triplets at room temperature (see section IVA), such as pentacene,<sup>19</sup> tetracene,<sup>22</sup> and anthracene<sup>21</sup> in single crystal environment in contrast to low temperature ENDOR experiments. ESEEM also enables us to examine the hyperfine interaction of organic triplets in randomly oriented samples<sup>18</sup> as demonstrated in section IVB. So ESEEM has much more to offer than ENDOR. However, the ESEEM technique is again limited by the instrument deadtime and intrinsic phase memory time of the concerned triplet state. When the phase memory time is shorter than or equal to the instrument deadtime ( $\sim 200$  ns), not much useful ESEEM can be obtained. Fortunately, the instrument deadtime has gradually been improved as indicated at the end of the last section. On the other hand, the phase memory time can be lengthened by lowering the sample temperature and dispersing the triplet of interest in different solvent or host crystal, such as perdeuterated compounds.

Recently, van der Poel et al. applied the combination of ESE and ENDOR techniques, spin echo ENDOR (pulsed ENDOR), to study the hyperfine structure of the interior protons of free-base porphine in its lowest photoexcited triplet state.<sup>44</sup> The sensitivity of spin-echo-ENDOR technique is claimed to be more than 1 order of magnitude greater than the conventional ENDOR. Thus, the spin echo ENDOR certainly has much to offer in years to come.

In summary, the ESE spectroscopy is a superior technique for studying both the time domain and frequency domain behaviors of organic triplets.

### VII. Concluding Remarks

The advent of high-power laser, pulsed-high-power microwave sources, fast digitizing equipment, and computer facilities have made the ESE technique an accessible and viable tool for the study of triplet states at ambient temperature. The fast detection scheme of the technique allows us to perform experiments on short-lived and fast relaxing triplets. The time-resolved

nature of the ESE technique can provide us with the triplet spin dynamics, such as relaxation processes, spin polarization, triplet population, decay kinetics, and excitonic motion. The intense microwave pulse used in an ESE experiment often changes the magnitude and direction of the effective field seen by nuclei. The change of effective field can give rise to a coherent superposition of nuclear spin states which evolves in time at frequencies corresponding to ENDOR frequencies. Thus, the coherent effect yields HF tensor elements and the detailed spin density distribution of the triplet. Furthermore the presence of the magnetoselection effect enables us to employ the ESE technique to study samples in rigid glasses or powdered solids. The ability to work with randomly oriented samples and yet still be able to extract anisotropic information about the relaxation processes and ENDOR frequencies should prove its great value in the near future, especially for systems where the preparation of single crystal is very difficult if not impossible, such as biological systems and some macromolecules. We should point out the triplet state is a natural built-in "spin label" which enables us to probe the electronic structure of the system of interest in an unperturbed manner. One may further utilize the triplet as a spin probe to study the structure and dynamics of polymers and other biological systems.

*Acknowledgments.* I wish thank Hsiang-Lin Yu and David J. Sloop for their contribution to part of the work I described here. Part of the work presented here was done at Argonne National Laboratory where I spent a pleasant year (1980–1981) in James R. Norris' laboratory. Helpful discussion with Norris and technical assistance from him and members of his group, especially Michael K. Bowman are gratefully acknowledged. Collaboration and discussion with Sam I. Weissman have been the most fruitful and rewarding aspects of carrying out this project. This work was supported by the donors of the Petroleum Research Fund, administered by the American Chemical Society, and the National Science Foundation, Solid State Chemistry (DMR-8205422).

### VIII. References

- (1) Hutchison, C. A., Jr.; Mangum, B. W. *J. Chem. Phys.* **1958**, *29*, 952; **1961**, *34*, 908.
- (2) Hutchison, C. A., Jr. "The Triplet State"; Zahlen, A. D., Ed.; Cambridge University Press, New York, 1967; p 63.
- (3) Kwiram, A. L. "International Review of Science"; Butterworths: London, 1972; Physical Chemistry Series One, Vol. 4, p 271 and references therein.
- (4) Hochstrasser, R. M. "International Review of Science"; Butterworths: London, 1976; Physical Chemistry Series Two, Vol. 3, p 1 and references therein.
- (5) El-Sayed, M. A. *Annu. Rev. Phys. Chem.* **1975**, *26*, 235–258.
- (6) Levanon, H.; Norris, J. R. *Chem. Rev.* **1978**, *78*, 185.
- (7) Schmidt, J.; van der Waals, J. H. "Time Domain Electron Spin Resonance"; Kevan, L., Schwartz, R. N., Ed.; Wiley-Interscience: New York, 1979; p 343 and references therein.
- (8) McGlynn, S. P.; Azumi, T.; Kinoshita, M. "Molecular Spectroscopy of the Triplet State"; Prentice-Hall: Englewood Cliffs, NJ, 1969.
- (9) Clarke, R. H., Ed. "Triplet State ODMR Spectroscopy"; Wiley-Interscience: New York, 1982.
- (10) Norris, J. R.; Thurnauer, M. C.; Bowman, M. K. "Advances in Biological and Medical Physics"; Academic Press; New York, 1980; Vol. 17, p 316–415.
- (11) Mims, W. B. "Electron Paramagnetic Resonance"; Geschwind, S., Ed.; Plenum: New York, 1972; p 263–351 and references therein.
- (12) Kevan, L.; Schwartz, R. N., Ed. "Time Domain Electron Spin Resonance"; Wiley-Interscience: New York, 1979.

- (13) Weissman, S. I. *Annu. Rev. Phys. Chem.* **1982**, *33*, 301.  
(14) Botter, B. J.; Doetschman, D. C.; Schmidt, J.; van der Waals, J. H. *Mol. Phys.* **1975**, *30*, 609.  
(15) Bowman, M. K.; Norris, J. R. *J. Chem. Phys.* **1982**, *77*, 731.  
(16) Cheng, C.-P.; Lin, T.-S.; Sloop, D. J. *Chem. Phys. Lett.* **1976**, *44*, 576.  
(17) Doetschman, D. C.; Fierstein, E. S.; Michaelis, J.; Desantolo, A. M.; Utterback, S. G. *Chem. Phys. Lett.* **1980**, *74*, 539.  
(18) Lin, T.-S.; Bowman, M. K.; Norris, J. R.; Closs, G. L. *Chem. Phys. Lett.* **1981**, *78*, 283.  
(19) Sloop, D. J.; Yu, H.-L.; Lin, T.-S.; Weissman, S. I. *J. Chem. Phys.* **1981**, *75*, 3746.  
(20) Yu, H.-L. Ph.D. Thesis, Washington University, 1982.  
(21) Yu, H.-L.; Sloop, D. J.; Weissman, S. I.; Lin, T.-S.; Norris, J. R.; Bowman, M. K. *J. Phys. Chem.* **1982**, *86*, 4287.  
(22) Yu, H.-L.; Lin, T.-S.; Sloop, D. J. *J. Chem. Phys.* **1983**, *78*, 2184.  
(23) Schmidt, J. *Chem. Phys. Lett.* **1972**, *14*, 411.  
(24) Breiland, W. G.; Harris, C. B.; Pines, A. *Phys. Rev. Lett.* **1973**, *30*, 158.  
(25) Botter, B. J.; Nenhof, C. J.; Schmidt, J.; van der Waals, J. H. *Chem. Phys. Lett.* **1976**, *43*, 210.  
(26) Botter, B. J.; van Strien, A. J.; Schmidt, J. *Chem. Phys. Lett.* **1977**, *49*, 39.  
(27) van Strien, A. J.; Schmidt, J. *Chem. Phys. Lett.* **1980**, *70*, 513.  
(28) Botter, B. J.; Doetschman, D. C.; Schmidt, J.; van der Waals, J. *Chem. Phys. Lett.* **1976**, *38*, 18.  
(29) Clarke, J. R.; Hutchison, C. A., Jr. *J. Chem. Phys.* **1971**, *54*, 2962.  
(30) Grivet, J. R. *Chem. Phys. Lett.* **1969**, *4*, 104.  
(31) Haarer, D.; Schmidt, D.; Wolf, H. C. *Phys. Stat. Sol.* **1967**, *23*, 633.  
(32) Amos, A. T. *Mol. Phys.* **1962**, *5*, 91.  
(33) Coulson, C. A.; Streitwieser, A., Jr. "A Dictionary of  $\pi$ -Electron Calculations"; Pergamon: New York, 1965.  
(34) Scott, T. A. *J. Chem. Phys.* **1962**, *36*, 1459.  
(35) Lin, T.-S.; Norris, J. R.; Bowman, M. K., unpublished results.  
(36) Grebel, V.; Levanon, L. *Chem. Phys. Lett.* **1980**, *72*, 218.  
(37) Kooter, J. A.; van der Waals, J. H. *Mol. Phys.* **1979**, *37*, 997.  
(38) Kooter, J. A.; van der Waals, J. H.; Knop, J. V. *Mol. Phys.* **1979**, *37*, 1015.  
(39) Yu, H.-L.; Sloop, D. J.; Lin, T.-S., to be published.  
(40) Kim, S. S.; Weissman, S. I. *J. Magn. Reson.* **1976**, *24*, 167.  
(41) Clarke, R. H.; Frank, H. A. *J. Chem. Phys.* **1976**, *65*, 39.  
(42) Kim, S. S.; Weissman, S. I. *Rev. Chem. Intermed.* **1979**, *3*, 107.  
(43) Davis, J. L.; Mims, W. B. *Rev. Sci. Instrum.* **1981**, *52*, 131.  
(44) van der Poel, W. A. J. A.; Singel, D. J.; Schmidt, J.; van der Waals, J. H. *Mol. Phys.* **1983**, *49*, 1017.